Control Engineering Practice 18 (2010) 904–917

Contents lists available at ScienceDirect

Control Engineering Practice

journal homepage: www.elsevier.com/locate/conengprac

Hybrid modeling and identification of dry friction systems, application to a clutch actuator

Rémy Nouailletas [a,*], Eduardo Mendes [a], Damien Koenig [b]

[a] LCIS, Institut Polytechnique de Grenoble, ESISAR, EA 3747, 50 rue Laffemas, BP 54, 26902 Valence, France
[b] GIPSA, Institut Polytechnique de Grenoble, UMR 5528 CNRS-INPG-UJF, BP 45, 38402 Saint Martin d'Hères, Cedex, France

ARTICLE INFO

Article history:
Received 5 May 2009
Accepted 26 March 2010
Available online 18 April 2010

Keywords:
Dry friction
Hybrid modeling
Identification
Clutch actuator
Stick–slip
Limit cycle

ABSTRACT

This paper proposes a new general framework, i.e. hybrid modeling, to model dry friction systems. The proposed hybrid model has two modes (states): one models the system sliding, the second the system sticking. The model's main advantage is the adaptation capability to observable phenomena. It is shown for the most common behaviors encountered experimentally and comparisons with other models presented in the literature are carried out. The models and methods of parameters identification of the literature are generally validated experimentally on system with sensors and actuators of high precision. This paper focuses on modeling and identifying complex mechanical system with low resolution sensors. The presented theoretical work is validated experimentally on a clutch-by-wire.

1. Introduction

Friction exists in mechanical systems where relative motion occurs between mechanical parts. The various friction components are dissipative terms, they generally stabilize naturally the system in open loop but on the contrary they lead to lower precision in closed loop and limit cycles may occur around the desired equilibrium. Due to this, frictions modeling should be done carefully (Alpeter, 1999; Armstrong-Helouvry, Dupont, & Canudas de Wit, 1994). For complex mechanical systems, the development time of an accurate (validated simulation and physical parameters values) process model with an account of friction can be long. Although the physical phenomena implied in friction are generally well understood, all should not be taken into account for the modeling of the system or the synthesis of the system control law. The designer has to choose the precision of the model as a function of the control objectives and of the available sensors with given precision. Then, it is of practical interest to have a general framework for the modeling of frictions according to the particular objective.

The surface of a solid is rough: microscopic artefacts draw a random map of holes and bumps. If solids are in contact, frictions appear at the interface when one has relative motion with respect to the other: energy is dissipated by the shocks between the asperities of both surfaces. A friction force opposed to the movement models this dissipation (Al-Bender & Swervers, 2008). When the system is motionless, adhesions exist between the two surfaces. These adhesions may be deformed like a spring by small applied forces parallel to the surfaces. If the breakaway force is reached, the rupture of the adhesion causes a sliding movement (Canudas de Wit, Olsson, Astrom, & Lischinsky, 1995).

Following these simple descriptions, many works have been done to detail friction phenomenon. The macroscopic behavior of systems submitted to friction can be summed up into seven properties:

- *Stiction*: The solids do not slip as much as the microscopic liaisons are not broken. The rupture occurs when the breakaway force (equal to the Coulomb force) is applied to the system.
- *Rising static friction*: The breakaway force is function of the dwell time.
- *Frictional memory*: For low velocities, a delay appears between the variations of the speed and ones of the friction (dynamics of the lubrication fluid).
- *Pre-sliding displacement* (Canudas de Wit et al., 1995): When the system is stuck, adherences have an elastic behavior.
- *Stribeck effect* (Stribeck, 1902): For low velocities, friction force f as follows:

$$f(v(t)) = \left(f_c+(f_s-f_c)e^{-(v(t)/v_s)^{\delta_s}}\right)\ \mathrm{sign}(v) \tag{1}$$

* Corresponding author.
E-mail addresses: remy.nouailletas@lcis.grenoble-inp.fr, remy.nouailletas@gmail.com (R. Nouailletas), eduardo.mendes@lcis.grenoble-inp.fr (E. Mendes), damien.koenig@gipsa-lab.grenoble-inp.fr (D. Koenig).

0967-0661/$ - see front matter © 2010 Elsevier Ltd. All rights reserved.
doi:10.1016/j.conengprac.2010.03.014

where v, f_c and f_s are, respectively, the relative speed between the two surfaces, the Coulomb and Stribeck forces. δ_s is used to control the behavior of f near $v=0$. The decreasing speed of f from f_s to f_c is tuned with the Stribeck speed v_s.

- *Viscous friction*: For high velocities, friction force is proportional to the speed:

$$f(v(t)) = f_v v \tag{2}$$

f_v is the proportional coefficient of the *viscous friction*.

- *Hysteresis behavior with nonlocal memory* (Al-Bender & Swervers, 2008): In pre-sliding displacement, the adherences have not a linear behavior but follow a hysteresis function.

To model friction, the objective is to capture, depending on the system, the needed previous properties. First idea has been to propose static models following the sum of (1) and (2). Theoretically, *stiction* behavior is captured by these models. In practice, the discontinuity of the function sign needs to be smoothed to take into account simulation limits, loosing the *stiction* property. These models are a good alternative when only viscous friction (i.e. Eq. (1)) is modeled or when the speed sign does not change during the simulation.

Karnopp (1985) proposes to set the speed to 0 when *stiction* occurs. This model is a good solution to solve simulation convergence time problems, stick–slip cycles are well simulated but *stiction* is not exactly modeled.

To take into account complex phenomena as *pre-sliding displacement*, dynamic models have been introduced. A state z is added to model the average deformation of the stiction liaisons. Bliman and Sorine (1995) can be cited, but the reference model is the LuGre model (Canudas de Wit et al., 1995):

$$\dot{z} = v - \frac{|v|}{g(v)} z$$

$$\sigma_0 g(v) = f_c + (f_s - f_c) e^{-(v(t)/v_s)^{\delta_s}}$$

$$f = \sigma_0 z + \sigma_1 \dot{z} + f_v v \tag{3}$$

where σ_0 and σ_1 are used to set the stiffness of the model. f_c, f_s, v_s and δ_s keep the definition given in (1). With this model, only *hysteresis behavior with nonlocal memory* is not captured. An other problem is that in some conditions, the system can present a position drift, see Section 2.5. By adding two new parameters to the LuGre model, Armstrong has solved this problem (Dupont, Armstrong, & Hayward, 2000), but the elastoplastic model does not model the *hysteresis behavior with nonlocal memory* of the microscopic adherences. The solution has been found with the Leuven model (Lampaert, Swervers, & Al-Bender, 2002; Swevers, Al-Bender, Ganseman, & Projogo, 2000). The model remains based on the LuGre model. Eq. (3) is modified, specially the function $g(v)$ which is replaced by a function modeling the hysteresis.

With this last model, all the enumerated properties are captured and the divergence problem for small displacement is solved. In the other hand, more than eight parameters are used by the Leuven model.

The friction model should be chosen as a function of the most important properties of the system. The sensors and the sample time of the controller need to be taken into account: if a position sensor with low resolution is used, it is useless to model *pre-sliding displacement*.

In this paper, friction systems are seen as 'hybrid systems'. Witsenhausen (1976) was the first to introduce this term to define a system with continuous dynamics together with some transition sets. Since a lot of work have been presented in journals (Antsaklis, 2000; Antsaklis & Nerode, 1998; Morse, Panelides, Sastry, & Schumacher, 1999), proceedings (specially in 'hybrid systems: computation and control' (Alur, Henzinger, & Sontag, 1996; Antsaklis, Kohn, Nerode, & Sastry, 1995, 1997; Di Benedetto & Sangiovanni-Vincentelli, 2001; Grossman, Nerode, Ravn, & Rischel, 1993; Henzinger & Sastry, 1998; Lynch & Krogh, 2000; Maler & Pnueli, 2003; Tomlin & Greenstreet, 2002; Vaandrager & van Schuppen, 2000) and books (van der Schaft & Schumacher, 2000). Moreover, hybrid system theory has been already used to model dry friction for specific mechanical applications (Sedghi, 2003).

Here a general hybrid model of friction is presented, it can be easily adapted to the specifications of the studied system. It can be seen as a general framework to model friction. Two modes are used to model the friction: slip mode and stick mode. Each presented property can be added independently without changing all the model equations. So the hybrid model complexity can be adjusted easily as needed to fit the behavior of the real system.

The most significant advantage is that the simplest version of the hybrid model with five parameters has the no-drift property, i.e. the position stays bounded when the absolute value of the input force is bounded by the Stribeck force f_s. In comparison, with the elastoplastic LuGre-based model, eight parameters are needed to model this behavior.

The first section of the paper is dedicated to the development of the hybrid model. The simplest form without pre-sliding displacement is firstly presented. Simulation parameters tuning is given. Then, pre-sliding displacement is taken into account in the model. To end this section, an identification method is presented to find a set of parameters when low resolution position sensor is used. To validate the hybrid model, it is compared to the LuGre and the elastoplastic models.

The second section presents the application of the proposed model to the modeling of a clutch actuator. First, the description of the system is done. Secondly, an exhaustive model is presented. Then, simplifications are done to obtain a simplest one. The previously presented identification method is applied to the system. To finish this section, validation and limitations of the model are presented.

Finally, Section 4 concludes the paper.

2. A hybrid model for dry friction

2.1. Hybrid model without pre-displacement

Pre-displacements are microscopic motions that appear when, from standstill, an input force lower than the Stribeck force is applied to the system. It corresponds to the setting in tension of the system adherence. To observe them in practice, a very precise position sensor needs to be used. In most industrial applications, the used position sensors are not enough precise to detect them. In this section, a hybrid model for dry friction without taking into account pre-displacements are given. For that, let us consider a single-mass system

$$\dot{x}(t) = v(t)$$

$$m\dot{v}(t) = u(t) - f(t, v, x, \ldots) \tag{4}$$

where x is the position, v the speed, $u(t)$ the input force and the force f representing frictions which may depend on speed, position, etc. and parameters as wear, Coulomb's friction level, Stribeck parameter, etc. (Canudas de Wit et al., 1995). The friction f is often taken as follows:

$$f(v(t)) = \left(f_c + (f_s - f_c) e^{-(v(t)/v_s)^2}\right) \text{sign}(v) + f_v v(t) \tag{5}$$

where f_c and f_s are, respectively, Coulomb's and Stribeck forces. With (5), the magnitude of the input force needs to be higher than f_s to accelerate the system from standstill; when the speed v is much higher than v_s the friction tends to $f_c \text{sign}(v) + f_v v$.

The genesis of the model proposed in Nouailletas, Hoang Le, Mendes, & Koenig (2008) for systems with dry friction starts from a simple report that a mechanical system has two operating modes: it moves or it is motionless. This can be modeled as a finite state machine with two states: state 1, the system moves according to (4); and state 0, the system is motionless with model (6) that ensures that the speed converges quickly to zero. It is of interest to note that if the study needs it, Eq. (6) can be modified to model pre-displacements (see Section 2.4).

$$\dot{x} = v$$

$$\dot{v} = -p_0 v, \quad p_0 \gg 1$$

$$f = u \tag{6}$$

Fig. 1 summarizes the state machine. When condition $C_{0\to1}$ (respectively, $C_{1\to0}$) is true, the system switches from sub-model 0 (1) to sub-model 1 (0). Fig. 2 represents the input force $u(t)$ in X-coordinate and the speed $v(t)$ in Y-coordinate. This map illustrates the possible system evolutions. From positive (negative) speed, the system only switches to sub-model 0, if $u(t)$ is lower (higher) than f_c $(-f_c)$ and the speed $v(t)$ is lower (higher) than Σ $(-\Sigma)$. So the condition $C_{1\to0}$ of Fig. 1 is

$$C_{1\to0} : ((u<f_c) \text{ and } (0<v<\Sigma)) \text{ or } ((u>-f_c) \text{ and } (-\Sigma<v<0)) \tag{7}$$

This condition is different from the original version in Nouailletas, Hoang Le et al. (2008). Here, in order to agree with mapping of Fig. 2, (7) ensures that when the sign of the speed changes, the system state passes trough sub-model 0.

To go from mode 0 to mode 1, the absolute value of input force needs to be higher than the Stribeck force f_s

$$C_{0\to1} : |u|>f_s \tag{8}$$

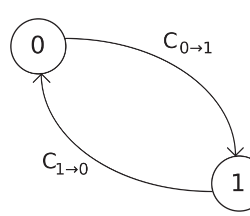

Fig. 1. State machine for dry friction modeling.

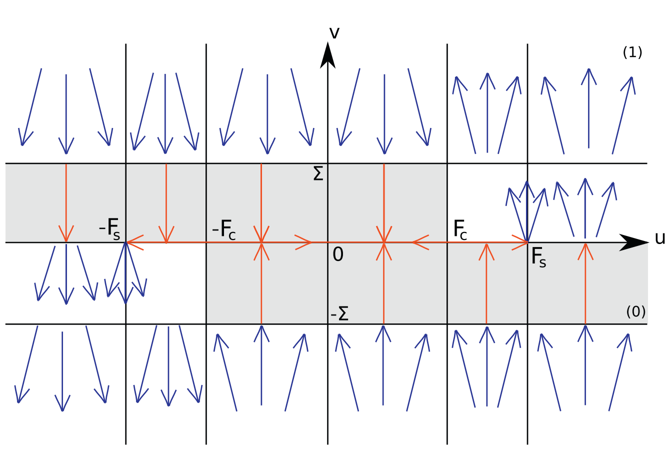

Fig. 2. Map of switches without pre-displacement, white zone: mode 1, light grey zone: mode 0.

2.2. Implementation and first tuning of the model

The previous subsection has presented an ideal hybrid model of system submitted to dry friction. In fact, ideally one has $p_0 \to +\infty$ and $\Sigma \to 0$. In this subsection, the numerical implementation of the proposed model taking into account the simulation time is addressed.

For numerical integration of a continuous time system, a variable time step method is usually recommended. Generally, the user can choose the maximum and minimum step time ($T_{e\ \max}$ and $T_{e\ \min}$) of the solver. Here, it is addressed the link between p_0, Σ and $T_{e\ \max}$.

With the proposed hybrid model the maximum step time $T_{e\ \max}$ should be chosen carefully: when speed changes sign, the model have to activate mode 0 before come back in mode 1. If the sample time T_e is too high, the speed can change sign during an integration step without becoming lower than Σ in absolute value. The model stays all the time in mode 1 in spite of the sign change. This problem appears with high accelerations. Neglecting friction forces in comparison with the input force, the maximal speed step between two time steps of the system solver is $u_{\max} T_{e\ \max}/m$. This speed step has to be lower than Σ to avoid this problem.

Ideally, parameter p_0 of mode 0 should be chosen as high as possible. Clearly, the dynamics of the motion determined by p_0 needs to be much faster than that of mode 1, but higher it will, higher will be the computation time. In practice, data coming from system sensors are sampled with sample time T_s. In mode 0, the system is supposed to be motionless, then when the system switches in mode 0, the speed convergence time to zero should be lower than T_s. The trajectory of $|v|$ when the system switches in mode 0 at time $t_{1\to0}$ is

$$|v(t_{1\to0}+t)| = \Sigma e^{-p_0 t} \tag{9}$$

To obtain an almost speed convergence at time $t_{1\to0}+T_s$, p_0 should be put equal to n/T_s (with $n \in \mathbb{N} \gg 1$). For example with $n=5$, $|v(t_{1\to0}+T_s)| \le 2\%\Sigma$.

In mode 0, the convergence time of the speed to zero is not null due to the finite value of pole p_0. To ensure that the speed value is sufficiently closed to zero before a switch to mode 1 occurs, condition $C_{0\to1}$ needs to be completed

$$C_{0\to1} : (|u|>f_s) \text{ and } (|v|<\Sigma_2) \tag{10}$$

where Σ_2 can be taken equal to $2\%=(100-98)\%$ of Σ in order to be coherent with the tuning of p_0.

In mode 0, the displacement of the system during the speed convergence to zero is bounded by Σ/p_0. Given a position sensor with precision δ_x, if one needs to model only measurable displacements with the given sensor, it is sufficient to set Σ lower than $p_0\delta_x$. Lower values of Σ will increase the simulation time.

Expression (11) summarize conditions on the simulation parameters.

$$p_0 > \frac{5}{T_s}$$

$$\Sigma < \delta_x p_0$$

$$m\Sigma > u_{\max} T_{e\ \max} \tag{11}$$

With this tuning, *stiction*, *Stribeck effect*, *viscous fiction* phenomena can be modeled and simulation results respect the description of the ideal model. Nevertheless, if the input force is not bounded, a limitation of the model appears: $m\Sigma$ can be lower than $uT_{e\ \max}$ and so problems occur when the sign of the speed changes. In practice, all real mechanical systems have bounded inputs, so a set of simulation parameters can be always found to verify condition (11).

2.3. Comparison with the LuGre model

Since the first description of the LuGre model in Canudas de Wit et al. (1995), a lot of works have been done based on this approach. It became one of the reference models to describe dry friction systems. In Canudas de Wit et al. (1995), series of tests were carried out to validate that model. The proposed hybrid model without account for pre-displacements is now compared with LuGre model. The first test intends to verify the capability of modeling slip–stick motion of the system. The second one exhibits the limit-cycles caused by friction in closed-loop. For both tests, friction f of the hybrid model is chosen equal to (5). Table 1 gives all the parameters needed to carry out the simulations (equal to the ones given in Canudas de Wit et al. (1995)). The following equation reminds the LuGre model.

$$m\dot{v} = u - f(z,v)$$

$$\dot{z} = v - \frac{|v|}{g(v)} z$$

$$f(z,v) = \sigma_0 z + \sigma_1 \dot{z} + \sigma_2 v$$

$$\sigma_0 g(v) = f_c + (f_s - f_c) e^{-(v(t)/v_s)^2} \quad (12)$$

2.3.1. Stick–slip motion

To test the slip–stick motion behavior of the model, an experimental setup given by Fig. 3 is proposed in Canudas de Wit et al. (1995). It is a simple mass system where the input force $u(t)$ is $K(y-x)$. As it can be seen on Fig. 4, the hybrid model does not fit perfectly with the LuGre model. But the overall behavior is good: when the force of the spring becomes higher than stiction force, the mass slides, the spring force comes then back lower to the Coulomb force and the system stops. The small difference between LuGre and hybrid model is because of the pre-displacement motion. If the bristle stiffness and damping parameters σ_0 and σ_1 of the LuGre model are increased ($\sigma_0 = 10^8$ and $\sigma_1 = \sqrt{10^8}$) to minimize pre-displacement effect, the hybrid model fits perfectly with the LuGre model.

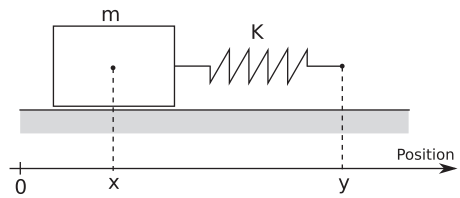

Fig. 3. Experimental setup to test the slip–stick motion effect.

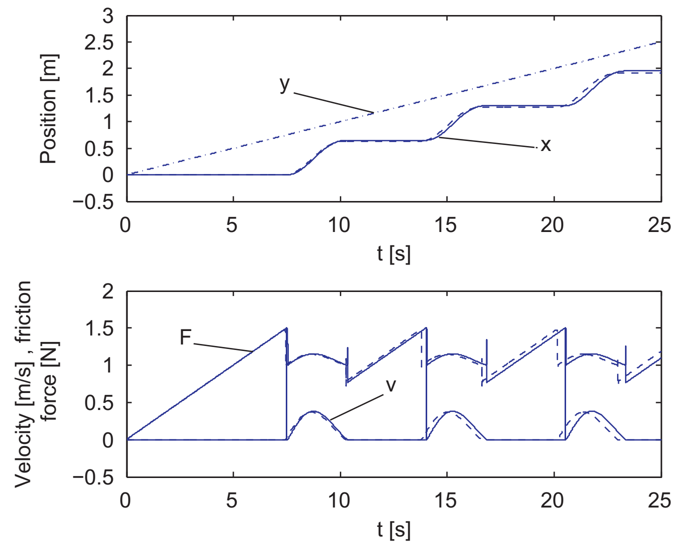

Fig. 4. Simulation ofslip–stick motion: LuGre model (dashed) and hybrid model (solid).

Table 1
Simulation parameters for validation tests.

	Value	Unit
Common parameters		
m	1	(kg)
f_c	1	(N)
f_s	1.5	(N)
v_s	10^{-3}	(m/s)
σ_2	0.4	(Ns/m)
$u_{\max}$	2	(N)
Slip–stick test parameters		
K	2	(N/m)
$\dot{y}$	0.1	(m/s)
PID parameters		
K_p	3	(N/m)
K_v	6	(Ns/m)
K_i	4	(N/m/s)
LuGre parameters		
σ_1	10^5	(N/m)
σ_0	$\sqrt{10^5}$	(Ns/m)
Hybrid parameters		
Σ	2×10^{-3}	(m/s)
$T_{e\ \max}$	10^{-3}	(s)
p_0	10^3	(rad/s)

2.3.2. Limit cycles caused by dry friction

A special behavior of systems submitted to dry friction appears when a position feedback control is used: the system does not converge to the right value but limit cycle oscillations may occur around it. To validate this behavior the same test as in Canudas de Wit et al. (1995) is done: A PID controller given by (13) is added to control the simple mass studied system. The simulation parameters are given by Table 1, the desired position is noted x_d.

$$u = -K_p(x-x_d) - K_v v - K_i \int (x-x_d)\, dt \quad (13)$$

Fig. 5 shows the obtained results. The transient response of the hybrid model fits well the transient response of the LuGre model. When limit cycles occur, the amplitude and the profile of the oscillations of the hybrid model is the same as with the LuGre one but the period is longer. This difference is due to the pre-displacement motion effect modeled by the LuGre model and not by the hybrid one. Again, if parameters σ_0 and σ_1 are increased in order to decrease the pre-displacement motion effect, both models perfectly fit.

Note that the simulation time of both models are very close one to the other.

2.4. Hybrid model with linear pre-sliding displacement

In the previous two subsections, since pre-sliding displacement has been neglecting, the differences between the presented

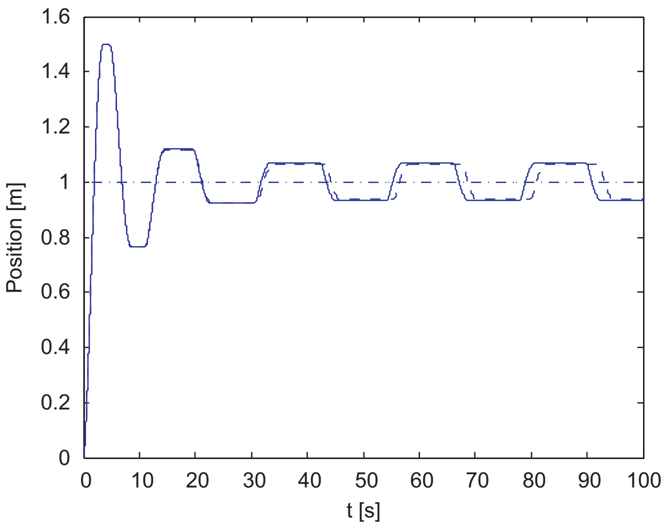

Fig. 5. Simulation of position feedback control: desired position (point-dashed), LuGre model with $\sigma_0 = 10^5$ and $\sigma_1 = \sqrt{10^5}$ (dashed) and hybrid model (solid).

model and the LuGre model have been observed. To take into account this effect in the hybrid model, one has only to modify Eq. (6) of mode 0.

When the system is motionless, adhesion appears between the mobile and the frame. This adhesion can be modeled as a force f_0 of a linear spring with damping and the pre-displacement by a new state z. In mode 0, the position of the system is equal to $x_{1\to 0}+z(t)$ where $x_{1\to 0}$ is the system position when it switches from mode 1 to mode 0. When adhesions are broken, i.e. when $|z(t)|$ is higher than a maximal pre-displacement $z_{\max}$, the system switches in motion mode. To take into account this behavior, the system model in mode 0 becomes

$$x(t) = x_{1\to 0}+z(t)$$

$$v(t) = \dot{z}$$

$$m\ddot{z} = u(t)-f_{stick}$$

$$f_{stick} = k_2\dot{z}+k_1 z \tag{14}$$

Condition (8) to switch from mode 0 to 1 is replaced by

$$C_{0\to 1} : ((z>z_{\max}) \text{ and } (u>f_s)) \text{ or } ((z<-z_{\max}) \text{ and } (u<-f_s)) \tag{15}$$

If $u(t)$ is null, (14) is very close to (6). In this case, $v(t)$ and $x(t)$ converge, respectively, to 0 and $x_{1\to 0}$.

In mode 1, adhesions have been broken and z is frozen. Conditions to switch from mode 1 to mode 0 remain but, Eq. (14) needs to be initialized, $\dot{z}_{1\to 0}$ is set equal to $\dot{v}_{1\to 0}$.

The above modification implies the introduction of three new parameters: $z_{\max}$, k_1 and k_2. $z_{\max}$ has a physical signification and can be easily experimentally measured. It will be show now that with some simple considerations k_1 and k_2 are easy to tune.

Static gain between $z(t)$ and $u(t)$ is equal to $1/k_1$. When $|u(t)|$ is equal to f_s, adhesions are broken and the system slides, so it minds that z is equal to $z_{\max}$. It comes easily

$$k_1 = \frac{f_s}{z_{\max}} \tag{16}$$

To tune k_2, the transfer function $H_{zu}(s)$ between z and u needs to be written

$$\frac{Z(s)}{U(s)} = H_{zu}(s) = \frac{1/k_1}{\dfrac{m}{k_1}s^2+\dfrac{k_2}{k_1}s+1}$$

$$H_{zu}(s) = \frac{G}{\dfrac{s^2}{w_0^2}+\dfrac{2\xi}{w_0}s+1} \tag{17}$$

where G is the static gain of the H_{zu}. w_0 is set by f_s and $z_{\max}$ and equal to $\sqrt{k_1/m}$, ξ is the damping coefficient set arbitrary to 1, in order to obtain well-behaved stick–slip transitions, during simulations (Canudas de Wit, 1999). So it comes easily the value of k_2

$$k_2 = 2\sqrt{\frac{mf_s}{z_{\max}}} \tag{18}$$

With the proposed tuning method of k_1 and k_2 by Eqs. (16) and (18), addition of pre-sliding effect to the switched model adds just one new parameter $z_{\max}$ that can be directly measured experimentally if the available position sensor has enough precision to account for pre-displacement: for small speed, the term $k_2\dot{z}$ is neglected and the friction force f_{stick} is proportional to z, so the rupture between the two modes can be observed and the parameter $z_{\max}$ can be read on the plan (x,u) (Dupont, Hayward, Armstrong, & Altpeter, 2002).

2.5. Comparison with other models of the hybrid model to model pre-sliding displacement

To model pre-sliding displacement, many models have been proposed. Dahl and LuGre models (which is a generalization of the Dahl one) are widely used. Fig. 6 shows the pre-sliding displacement z as a function of the system position x. $\dot{x}_{1\to 0}$, the initial speed, is equal to 0, $z_{\max}$ is set to 10^{-5} m, the other parameters are given by Table 1. The Dahl model is a Lugre one where the Stribeck force f_s and the parameter σ_0 are equal, respectively, to the Coulomb force f_c and zero. The hybrid model fits very well with the Lugre model (considered as the reference model). Dahl model is a good approximation (but Stribeck effect is not modeled). Pre-displacement with the LuGre model presents an overshoot which is undesired.

Dahl and LuGre models show position drift in some conditions. This is due to the fact that these models does not model accurately stiction behavior. In Dupont et al. (2000), the Armstrong model proposes a modification of the LuGre model to solve this problem. A function $\alpha(z)$ is added to limit pre-sliding

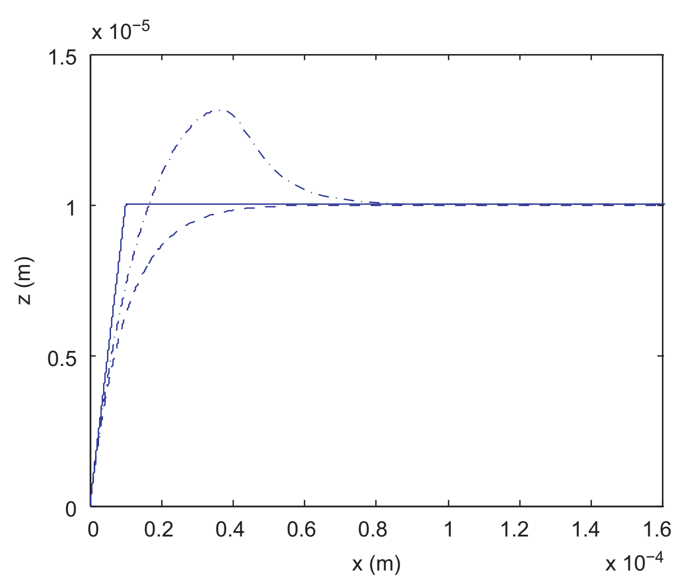

Fig. 6. Pre-sliding displacement: hybrid model (solid) equivalent to the theoretical real trajectory, Dahl model (dashed), LuGre model (point dashed).

displacement between $z_{\max}$ and $-z_{\max}$. To tune this function, two new parameters have to be defined: $z_{\max}$ and z_{ab}. $z_{\max}$ has the same definition as with the hybrid model, while z_{ab} takes a value slightly smaller than $z_{\max}$.

The proposed hybrid model naturally permits to model accurately pre-displacement as it is shown in Figs. 7 and 8. The used test which is very close to the one proposed in Dupont et al. (2000), is also applied to the LuGre and Armstrong models. Simulation and model parameters are given by Table 2. The position given by the LuGre model diverges but position given by Armstrong and hybrid models stay between 0 and $z_{\max}$ and are very closed. More z_{ba} is closed to $z_{\max}$, more the Armstrong position is closed to the hybrid model position.

2.6. Modeling other friction phenomena

The proposed hybrid model for pre-sliding displacement is simple since the adherences are modeled by a linear spring. Following the introduction reminder, three properties are not taken into account with this model: *rising static friction*, *frictional memory* and *hysteresis behavior with nonlocal memory*. Each of these behaviors can be added easily and independently to the proposed hybrid model by modifying (14) and/or (15).

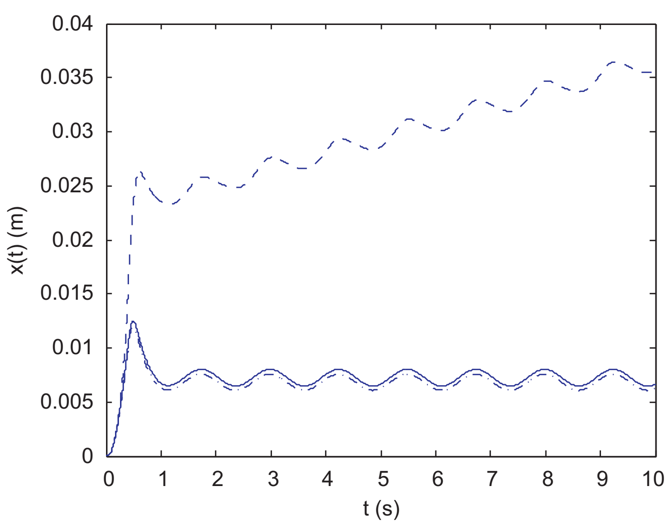

Fig. 7. Drift test: hybrid model (solid), LuGre model (dashed), Armstrong model (point dashed).

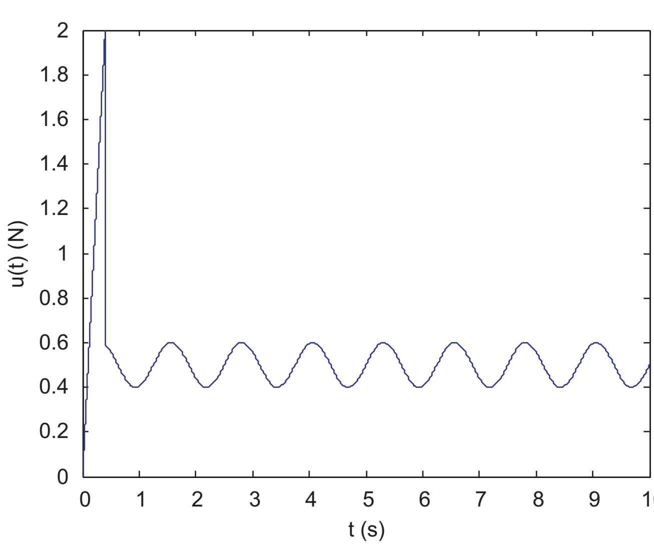

Fig. 8. Used input force for the drift test.

Table 2
Simulation parameters for pre-sliding tests.

	Value	Unit
Common parameters		
m	1	(kg)
f_c	1	(N)
f_s	1.1	(N)
v_s	0.1	(m/s)
σ_2	0	(Ns/m)
$z_{\max}$	0.01	(m)
LuGre and Armstrong parameters		
σ_1	$\frac{f_s}{z_{\max}}$	(N/m)
σ_0	$2\sqrt{\frac{mf_s}{z_{\max}}}$	(Ns/m)
z_{ba}	0.009	(m)
Hybrid parameters		
Σ	10^{-4}	(m/s)
$T_{e\ \max}$	10^{-3}	(s)

First, the phenomenon of *frictional memory* is the dynamics of the adhesions for low velocities. These dynamics are modeled by Eq. (14). Mass m may be modified in mode 0 to adjust the desired behavior.

Second, to take into account the *rising static friction* property, one has to modify f_s as a bounded function of t and reset it to its minimal value at each switch from mode 1 to mode 0. Note that any existing models take into account explicitly this behavior.

Third, for the *hysteresis behavior with nonlocal memory* of friction during sticking mode, f_{stick} should be modified to a nonlinear function of z and $\dot{z}$. In Lampaert et al. (2002) and Swevers et al. (2000), two functions are proposed. Note that also a Preisach model may be used (Mayergoyz, 1991).

Finally, the proposed hybrid model is able to be adapted to model friction properties. In this paper, some answers have been given to tune it for a basic modeling of pre-sliding displacement. Advanced sticking properties can be added and tuned using results of other models (Canudas de Wit, 1999).

2.7. Summary

Two versions of the hybrid model for dry friction system have been presented. The first one does not model the predisplacement

- Mode 0:

$$\dot{x} = v$$

$$\dot{v} = -p_0 v$$

$$f = u \tag{19}$$

- Mode 1:

$$\dot{x} = v$$

$$m\dot{v} = u - f(v) \tag{20}$$

The following simple friction function f can be chosen

$$f(v) = f_c sign(v) - f_v v \tag{21}$$

The conditions to switch between the two modes (sticking mode 0 and slipping mode 1) are

$$C_{1\to 0} : ((u < f_c) \text{ and } (v < \Sigma)) \text{ or } ((u > -f_c)) \text{ and } (u > -\Sigma)) \tag{22}$$

$$C_{0\to 1} : (|u| > f_s) \text{ and } (|v| < \Sigma_2) \tag{23}$$

The parameters are divided in physical parameters (m,f_c,f_v and f_s) and simulation parameters (Σ, Σ_2, p_0). These ones need to check the followings inequalities:

$$\Sigma_2 < \Sigma$$

$$p_0 > \frac{5}{T_s}$$

$$\Sigma < \delta_x p_0$$

$$m\Sigma > u_{\max} T_{e\ \max} \tag{24}$$

where T_s is the sampling time of the control system and $T_{e\ \max}$ is the maximal integration time used by the simulation solver.

The second version models the pre-displacement as a linear spring with a damping coefficient, only the sticking mode and the switching condition $C_{0\to1}$ are modified

$$x(t) = x_{1\to0} + z(t)$$

$$v(t) = \dot{z}$$

$$m\ddot{z} = u(t) - f_{stick}(z)$$

$$f_{stick}(z) = k_2\dot{z} + k_1 z \tag{25}$$

$$C_{0\to1} : ((z > z_{\max}) \text{ and } (u > f_s)) \text{ or } ((z < -z_{\max}) \text{ and } (u < -f_s)) \tag{26}$$

where $z_{\max}$ is the value of maximal pre-displacement. The condition on $T_{e\ \max}$ remains, the parameters k_1 and k_2 are defined by

$$k_1 = \frac{f_s}{z_{\max}}$$

$$k_2 = 2\sqrt{\frac{mf_s}{z_{\max}}}$$

$$m\Sigma > u_{\max} T_{e\ \max} \tag{27}$$

To take into account more complex behaviors of pre-displacement, only the function f_{stick} has to be modified.

3. Simple experimental identification methodology of friction parameters

3.1. The parameters to be identified

The main advantage of the presented hybrid model is that its complexity can be adapted to fit with the observable phenomena of the particular studied system. Then, only relevant parameters are used to model the experimental behavior. The case where the pre-displacement cannot be taken into account because of the low resolution of the position sensor is considered. Then, the sticking mode (mode 0) is modeled by (6), and when the model is in mode 1, the Stribeck effect is supposed inobservable. The dynamic equation becomes

$$\dot{x} = v$$

$$m\dot{v} = u - f_v v - f_c\ \text{sign}(v) \tag{28}$$

From (28) and $C_{0\to1}$, given by (10), it comes the minimum set of parameters to be identified (m,f_c,f_v,f_s). Parameters (p_0,Σ,$T_{e\ \max}$) are easily obtained by checking inequalities (11) defined in Section 2.2.

Many works proposed an advanced algorithms and methods to identify the set of parameters of dry friction models (Alpeter, 1999; Besancon-Voda & Besancon, 1999; Besancon-Voda & Blaha, 2002; Canudas de Wit, 1999). In Nouailletas, Mendes, & Koenig (2008) a least square algorithm using an assessment of power is proposed to identify the parameters of (28) without having difficult tuning of filters of measured quantities. Due to the low resolution of the position sensor, maximum speed limitation, etc., in many practical industrial cases, the use of these methods is very difficult or impossible. In this section, identification of the needed parameters of the system submitted to these constraints of low resolution of position sensor is proposed. A simple but robust methodology is given to quickly find a set of parameters for the hybrid model without predisplacement modeling. Particular attention is given to the noise from the sampling of the data. The proposed method can be seen as a first rough estimation of the model parameters. In most of industrial situations it will be sufficient because parameters change with time and robust control is needed. If higher precision of parameters determination is needed and if the data acquisition system allows it, advanced methods can be applied with first using the proposed identification method in order to initialize the parameters.

The noise involved in the identification algorithm is mainly because of the numerical derivation of the measured position x_s to obtain the discrete time estimated speed v_s and acceleration a_s, as given by

$$v_s(k) = \frac{x_s(k) - x_s(k-1)}{T_s}$$

$$a_s(k) = \frac{x_s(k) - 2x_s(k-1) + x_s(k-2)}{T_s^2} \tag{29}$$

where T_s is the sampling time. One can evaluate the effect of the resolution of the position sensor δ_x on v_s and a_s. For that, an upper bound of the absolute values of the errors between real and estimated v_s and a_s can be given as

$$\Delta v = \frac{\delta_x}{T_s}$$

$$\Delta a = \frac{2\delta_x}{T_s^2} \tag{30}$$

In (28), the mass m is coupled to the acceleration term a_s which is the most noisy because of the term T_s^2 from (30). The maximal acceleration $a_{\max}$ is bounded by the ratio $u_{\max}/m$. The ratio between the acceleration a_s and the noise Δa is bounded then by $T_s^2 u_{\max}/2m\delta x$. If this term is too small, the acceleration signal is too noisy to obtain good identification of the mass. To define the limit between a good and a bad signal to noise ratio, it is interesting to search the equivalent uncertainty Δm:

$$m(a + \Delta a) = (m + \Delta m)a$$

$$\Delta m = m\frac{\Delta a}{a}$$

$$\Delta m = \frac{2m^2\delta x}{T_s^2 u_{\max}} \tag{31}$$

As in the following, if Δm is higher than the theoretical uncertainty on m, it is preferable to suppose m known with its bounded uncertainty Δm. In practice, m is usually well known thanks to the mechanical design of the system. The value of friction parameters are generally not well known because of uncertainty on lubrication wearing or manufacture surface default.

In the following, the case of a system with very low position sensor resolution but known mass m is considered. So, the parameters to be identified are f_c, f_v and f_s.

3.2. Identification of the breakaway force f_s

From standstill, if the input $u(t)$ is increased, a motion occurs when $u(t)$ is slightly higher than the breakaway force f_s. Based on this fact, a simple algorithm has been given in Nouailletas, Mendes, et al. (2008) to estimate f_s. The block diagram of this algorithm is reminded on Fig. 9. Experimentally, the input torque is slowly increased until a motion occurs, then the actual value of $u(t)$ is saved and is reset after. When the maximum position is reached, the identification is done again by decreasing the input torque to go back to the initial position. Several go and returns are done to obtain accurate mean values depending on the position.

After post-treatment of the obtained data in order to remove measurement artifacts, the identified positive and negative breakaway forces are averaged to give the identified breakaway force f_s.

3.3. Identification of parameters in mode 1

As said before, the mass m of the system is supposed to be known. Then, from (28) and (29), it comes

$$y(k) = (u_s(k) - m a_s(k))\ \mathrm{sign}(v_s(k)) = f_v |v_s(k)| + f_c \tag{32}$$

where $y(k)$ is the input signal of the identification algorithm. Suppose a sinusoidal speed $v_s(k)$ of the form

$$v_s(k) = V_0 \sin(2\pi f_0 T_e k)$$

then (32) becomes

$$\begin{aligned} y(k) &= (u_s(k) - m V_0 2\pi f_0 \cos(2\pi f_0 T_e k))\ \mathrm{sign}(V_0 \sin(2\pi f_0 T_e k)) \\ &= f_v |V_0 \sin(2\pi f_0 T_e k)| + f_c = y_0(k) \end{aligned} \tag{33}$$

$y_0(k)$ is cyclic with a frequency equal to $2f_0$, using data from $k=0$ to $k=(T_e/2f)n$, the mean value of $y_0(k)$ is obtained

$$\overline{y_0} = \overline{u_s \mathrm{sign}(v_s)} - m\overline{a_s \mathrm{sign}(v_s)} = f_v \overline{v_s} + f_c \tag{34}$$

By Fourier decomposition, the averages $\overline{a_s \mathrm{sign}(v_s)}$ and $\overline{v_s}$ are found equal, respectively, to 0 and $2V_0/\pi$. It can be noticed that choosing a sinusoidal form for $v_s(k)$, $\overline{y_0}$ is not affected by the uncertainty on m or by the quantified noise on a_s. Eq. (34) is simplified as follows:

$$\overline{y_0} = \overline{u_s \mathrm{sign}(v_s)} = f_v \frac{2V_0}{\pi} + f_c \tag{35}$$

A single sinusoidal test is not sufficient to find f_v and f_c. A second one is done with a different amplitude V_1. The frequencies f_0 and f_1 are chosen to prevent stick–slip phenomena. In this case f_v and f_c are equal to

$$\begin{pmatrix} f_v \\ f_c \end{pmatrix} = \begin{pmatrix} \frac{2V_0}{\pi} & 1 \\ \frac{2V_1}{\pi} & 1 \end{pmatrix}^{-1} \begin{pmatrix} \overline{y_0} \\ \overline{y_1} \end{pmatrix} \tag{36}$$

Precision can be improved by adding data couples $(\overline{y_i}, V_i)$ to formulation (36), cf. (37). Gradient or least square optimization is used to find the best set (f_v, f_c).

$$\begin{pmatrix} \overline{y_0} \\ \overline{y_1} \\ \vdots \\ \overline{y_i} \\ \vdots \\ \overline{y_m} \end{pmatrix} = \begin{pmatrix} \frac{2V_0}{\pi} & 1 \\ \frac{2V_1}{\pi} & 1 \\ \vdots & \vdots \\ \frac{2V_i}{\pi} & 1 \\ \vdots & \vdots \\ \frac{2V_m}{\pi} & 1 \end{pmatrix} \begin{pmatrix} f_v \\ f_c \end{pmatrix} \tag{37}$$

4. The studied system

4.1. Presentation and first modeling

The studied system is a clutch actuator with a compensator spring to assist the electrical motor, see Fig. 10. A hydraulic system is used to connect the clutch to the actuator: by means of a master piston, the actuator moves the slave piston of the clutch. The relations (38) give the force F_2 applied to the actuator as a function of the clutch force F_c, and the displacement x_c of the clutch depending of the actuator position x.

$$F_2(x) = \frac{S_m}{S_s} F_c(x_c)$$

$$x_c = \frac{S_m}{S_s} x \tag{38}$$

where S_m and S_s are, respectively, the section of the master and the slave pistons. F_c is the force delivered by the clutch and x is the position of the actuator. In the continuation, the inertia of the fluid is neglected compared to the others dynamics. Moreover, in the speed range of the system, the viscous friction added by the hydraulic system is neglected compared to the dry friction of the other mechanical parts. The electrical motor moves the master piston via a motor speed reducer and a toothed rack. In the rest of the paper, these two mechanical links are modeled by a single toothed rack with equivalent reduction ratio r and efficiency η. A mechanical play exists in the toothed rack, it is amplified by the motor speed reducer, so the motor *sees* a play of numerical value $\varrho = 3$ rad. This play does affect the identification of the parameters of the model. Indeed, for the Stribeck force identification using method 3.2, data during direction change are not used. For the identification of the mode 1 parameters, the influence of the mechanical play during direction change can be compared to the bias added by the Stribeck effect during Coulomb force identification (cf. Besancon-Voda & Besancon, 1999). In the studied case, the erroneous data added by direction change are

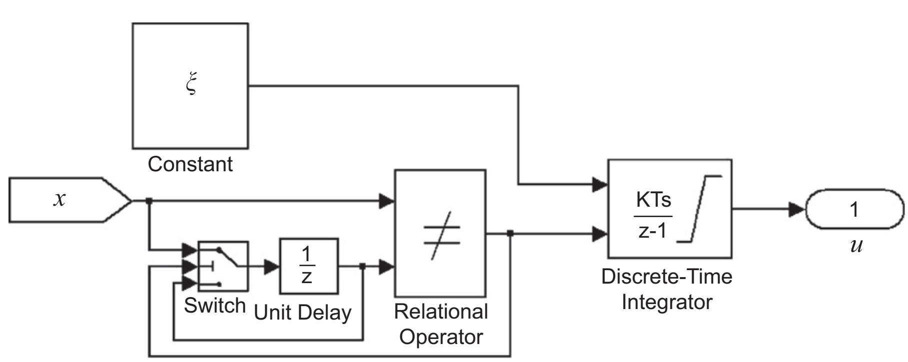

Fig. 9. Identification algorithm of the breakaway torque f_s.

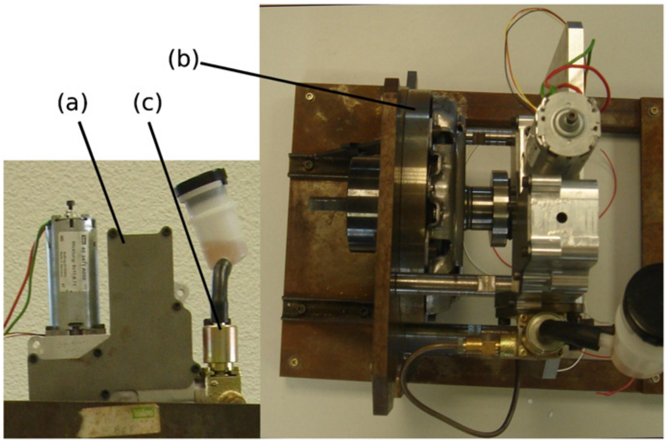

Fig. 10. Photos of the studied system (top and face): (a) actuator, (b) clutch and (c) hydraulic system.

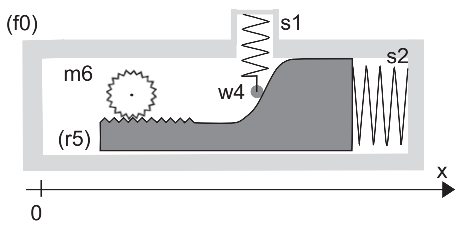

Fig. 11. Kinematic diagram of the studied system.

weak compared to the noise of the position sensor. Note that a method robust to this problem has been proposed in Nouailletas, Mendes, et al. (2008).

With (38), the clutch is modeled by a nonlinear spring acting directly on the actuator. Fig. 11 gives the kinematic diagram of the studied mechanical system with the used simplification hypotheses. It is composed of an electrical motor (m 6), a toothed rack (r 5), a compensator springs (s 1) and a spring (s 2) equivalent to the clutch. The spring (s 2) presses the toothed rack tangentially, spring (s 1) presses it via a little wheel of metal (w 4). The slope of the rack (r 5) is designed to compensate both springs: when spring (s 1) is compressed, spring (s 2) is uncompressed and conversely. Spring (s 1) applies a force F_1 perpendicularly to the translation axis of the rack. A force F_2 is produced by the spring (s 2). $u(t)$ is the motor torque. All the inertia and masses are negligible in front of the electrical motor inertia. The rack position $x(t) \in [0, x_{\max}]$ motion is given by

$$
\begin{aligned}
&\dot{x}(t) = r\upsilon(\omega)\omega(t)\\
&\dot{\theta}(t) = \omega(t)\\
&J\dot{\omega}(t) = u(t) - C_r(t)\upsilon(\omega) - C_d\\
&\upsilon(\omega) = sign\left(\frac{\varrho}{2} - \left|\int_{sat[-\varrho/2;\varrho/2]} \omega(t)\,dt\right|\right)
\end{aligned}
\tag{39}
$$

where ω is the speed of the motor, r the conversion ratio between rack position and motor angle, J the motor inertia and C_r the resistive torque due to all system resistive forces. The function $\upsilon(\omega)$ models the mechanical play. The measured output is the motor rotor position θ. This value is quantified with N_p points for 2π motor rotation.

C_r given by (40) is a function of the spring forces F_1 and F_2, and the friction F_f between the rack (r 5) and the frame (f 0). All the other frictions are negligible. The wheel (w 4) presses the rack (r 5) by means of a slope of angle $\alpha(x)$ with the axis (Ox).

$$
C_r(t) = \frac{1}{r\eta}(F_2(x) - F_1(x)\tan(\alpha(x)) + F_f(F_1, \dot{x}, u)) + C_d \tag{40}
$$

where η is the efficiency of the toothed rack link. The friction force F_f given by (41) represents viscous and dry frictions of the system. C_d is a friction torque added by the DC motor.

$$
F_f = F_c(1 + \sigma e^{-(\dot{x}(t)/v_s)^2})\ \mathrm{sign}(\dot{x}(t)) + F_v\dot{x}(t) \tag{41}
$$

F_f is supposed to be proportional to the force F_1 perpendicular to the rack. So, F_c and F_v which are, respectively, the Coulomb and viscous forces are equal to $\mu_c F_1(x)$ and $\mu_v F_1(x)$. v_s and σ are parameters to model Stribeck effect.

To ensure that the system is motionless for $x \in [0, x_{\max}]$ when the input force $u(t)$ becomes null, dry friction F_f needs to be enough high to compensate the spring forces residue $F_2 - F_1\tan(\alpha)$. Let define the following Lyapunov function:

$$
V(\dot{x}(t)) = \frac{J\dot{x}^2}{2r\eta} \tag{42}
$$

Neglecting viscous friction, which helps the system to stop, and after derivation of (42) along trajectories of (39), it comes

$$
\dot{V}(\dot{x}(t)) = \dot{x}(F_2(x) - F_1(x)\tan(\alpha(x)) - \mu_c(1+\sigma)F_1(x)\ \mathrm{sign}(\dot{x})) \tag{43}
$$

where (43) has to be negative definite when $\dot{x}(t) \neq 0$ to ensure that the equilibrium of (39) is at null speed:

$$
\mu_c > \frac{F_2(x) - F_1(x)\tan(\alpha(x))}{F_1(x)(1+\sigma)} \tag{44}
$$

If the force F_1 is never null, condition (44) for parameter μ_c ensures that for $u(t) = 0$, $\dot{x}(t) = 0$ is the equilibrium point of the system. So in practice, it minds that the spring (s 1) needs to be prestressed. Fig. 12 summarizes the springs characteristics. $F_1(x)$ and $\alpha(x)$ have been designed to compensate the spring force F_2. Note that if viscous frictions are not neglected, the stability condition (44) does not change because it is a steady state condition at null speed.

4.2. Model for identification and control purposes

The model presented in the last section is exhaustive and a lot of parameters need to be tuned. Most of them have a mechanical signification and are easily characterizable. But due to wear

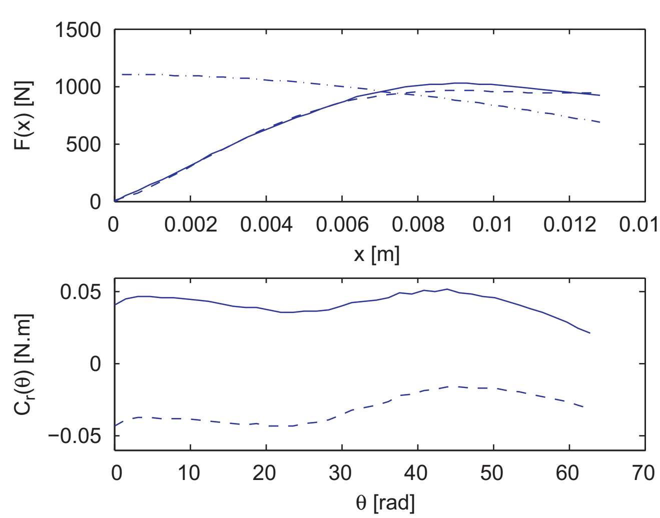

Fig. 12. Top: Forces function of the rack position: F_2 (solid), F_1 (point-dashed), $F_1\tan(\alpha)$ (dashed). Bottom: Resistive torques see by the motor: $\omega > 0$ (solid), $\omega < 0$ (dashed).

and/or process uncertainties, characteristics of elements as spring compensator or clutch may change. In the case of the studied system, interactions between elements make the identification of each one very difficult. Moreover, a so complex model is useless to design a controller. Then, such complete model is used to simulation purpose, and a simplest model has to be derived to control synthesis and experimental identification purposes.

Due to the reduction ratio, the play can be neglected: the expression $C_r(x)\upsilon(\omega)$ is replaced by $C_r(\theta)$. The error made for the calculation of C_r is neglected in front of the other approximations. Moreover, the measured position is θ, so in practice, there is no way to know the value of $\upsilon(\omega)$.

With a tuning of μ_c agreeing condition (44) and if viscous frictions are neglected, C_r has the same behavior as a dry friction torque. This remark allows to simplify (40) and only define C_r has a function of the rotor position and the speed sign. C_r is then approximated by two polynomial functions (for positive and negative speeds) fitting with the bottom graphics of Fig. 12. The generic dry friction model presented in the first part is used to implement model (39):

In mode 1:

$$\dot{x}(t) = r\omega(t)$$

$$J\dot{\omega}(t) = u(t) - C_r(\theta, \text{sign}(\omega))$$

$$\theta = \frac{x}{r}$$

$$C_r(\theta, \text{sign}(\omega) > 0) = a_3^+\theta^3 + a_2^+\theta^2 + a_1^+\theta + a_0^+$$

$$C_r(\theta, \text{sign}(\omega) < 0) = a_3^-\theta^3 + a_2^-\theta^2 + a_1^-\theta + a_0^-$$

In mode 0:

$$\dot{x}(t) = r\omega(t)$$

$$J\dot{\omega}(t) = -p_0\omega(t)$$

$$\theta = \frac{x}{r}$$

$$C_s(\theta, \text{sign}(u)) = \beta C_r(\theta, \text{sign}(u)) \quad (45)$$

C_r is a Coulomb friction torque depending on position. To switch from mode 0 to mode 1, the Stribeck effect is modeled by a resistive torque C_s proportional to and higher than C_r and opposed to the input torque, i.e. ω is replaced by u. Model parameters are given by Tables 3 and 4. Polynomial approximation on C_r can be viewed on Fig. 13. The proportional coefficient β between C_r and C_s will be identified in the next section. The simplest model of the clutch-by-wire is a mass submitted to friction function of the position θ. The behavior of this simple model has been validated in simulation (Nouailletas, 2009) and is closed to the real system as it will be shown in the following.

Table 3
Simple model parameters of the clutch actuator.

Parameters	Value	Unit
J	$1.32\times10^{-5}\pm2.1\times10^{-6}$	(kg/m)
r	2.0414×10^{-4}	( )
N_p	56	(pts/rotation)
Σ	150	(rad/s)
$T_{e\ max}$	10^{-3}	(s)
p_0	10^4	(rad/s)

Table 4
Parameters of the polynomial functions of C_r.

Parameters	Value	Parameters	Value
a_3^+	-9.466×10^{-7}	a_3^-	-1.009×10^{-6}
a_2^+	7.485×10^{-5}	a_2^-	8.743×10^{-5}
a_1^+	-8.790×10^{-4}	a_1^-	-9.314×10^{-4}
a_0^+	0.066	a_0^-	-0.050

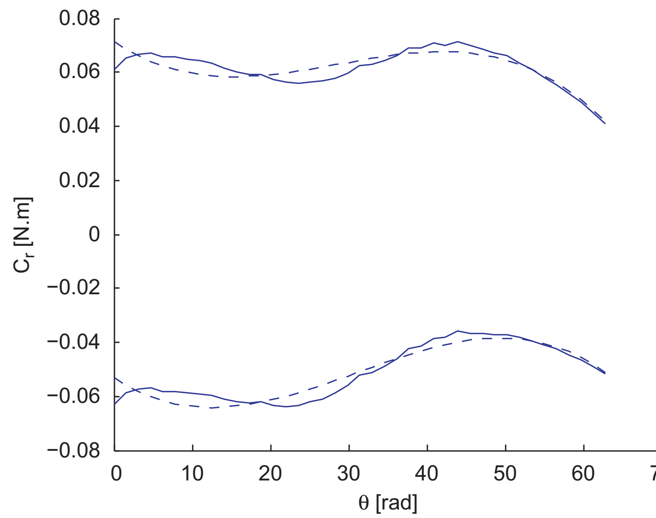

Fig. 13. Theoretical resistive torque (solid) and polynomial approximation (dashed).

5. Experimental identification of the test bench parameters

Due to unknown parameters as the prestressed value of the compensator spring (s1) or the real resistive force of the clutch (s2), the dry friction function given in the bottom view of Fig. 12 is different on the experimental test bench. Also, with the wearing of the oil, viscous friction that has been neglected can become important. So, a viscous friction torque equal to $f_v\omega(t)$ is added to the model. The inertia J can be theoretically calculated, but with the uncertainties on each mechanical piece, it can be different from the experimental one.

With these considerations, it appears that the simple model needs to be calibrated using identified parameters of the test bench. The hybrid model needs the knowledge of the parameters of each equation mode and each switching condition. To tune the equation of the mode 1 of the model described in the last section, the inertia J and the dry friction torque $\overline{C_r}$ are needed. A first approximation of theses parameters has been done.

In mode 0, the precision of the experimentally used position sensor is too weak to observe pre-displacements. So, model (6) is used for mode 0 and parameter p_0 is sufficient to tune this equation. To switch from mode 0 to mode 1, the Stribeck torque C_s needs to be identified. To switch from mode 1 to mode 0, the parameter Σ is needed. p_0 and Σ are tuned according to (11).

Finally, the parameters to be identified experimentally are J, f_v, C_r and C_s. First a simple test is practiced to determine the Stribeck torque as a function of the position and the sign of the speed. Then, to determine the inertia and the two friction parameters, dry friction is supposed constant. So that, it is the mean value $\overline{C_r}$ that is identified. Then using the mean value of C_s and according to the mechanical characteristics of the system, the Coulomb friction torque C_r is defined as follows:

$$C_r(\theta,\ \text{sign}(\omega)) = \frac{\overline{C_r}}{\overline{C_s}} C_s(\theta,\ \text{sign}(\omega)) = \frac{1}{\beta} C_s(\theta,\ \text{sign}(\omega)) \tag{46}$$

where it is supposed that C_s is proportional to C_r with gain β for all $\theta \in [0, \theta_{\max}]$.

5.1. Identification of the breakaway friction torque C_s

The test of Section 3.2 is used. Several go and returns are done to obtain accurate mean values depending on the position. Fig. 14 shows the experimental measurements. Note that the breakaway torque C_s is function of the position and the sign of the speed.

After post-treatment of the obtained data in order to remove measurement artifacts, the identified positive and negative Stribeck torques are fitted respectively by a polynomial function of degree 3 and 4 as a function of the position θ, see (47). Table 5 gives the obtained parameters of estimated polynomials and Fig. 15 shows the measured Stribeck torque values and corresponding fitting polynomials. The mean absolute values are $\overline{C_s^+} = 0.1352$ and $\overline{C_s^-} = 0.1506$ Nm, respectively, for positive and negative speeds.

$$C_s(\theta,\ \text{sign}(\omega) > 0) = b_3^+ \theta^3 + \cdots + b_0^+$$

$$C_s(\theta,\ \text{sign}(\omega) < 0) = b_4^- \theta^4 + b_3^- \theta^3 + \cdots + b_0^- \tag{47}$$

5.2. Identification of J, f_v and $\overline{C_r}$

The sample time of the acquisition system and the maximal input torque are, respectively, equal to 1 ms and 2 Nm. From Section 3.2, the ratio signal to noise for the acceleration is equal to $T_s^2 u_{\max}/2J\delta\theta$. With nominal values, this ratio equal to 0.68, is to small to expected a good identification of J. This bad ratio is equivalent to an uncertainty on J of 1.95×10^{-5} m^2 kg. This uncertainty is 10 times higher than the theoretical value of J (equal to 2.1×10^{-6} m^2 kg). So with the used acquisition system it is useless to identify the inertia J because excepted results can not be better than mechanical conception study.

The method of Section 3.2 is applied to the studied system. A controller is used to control the sinusoidal trajectory of the system for different speed amplitudes. From the results of Fig. 16,

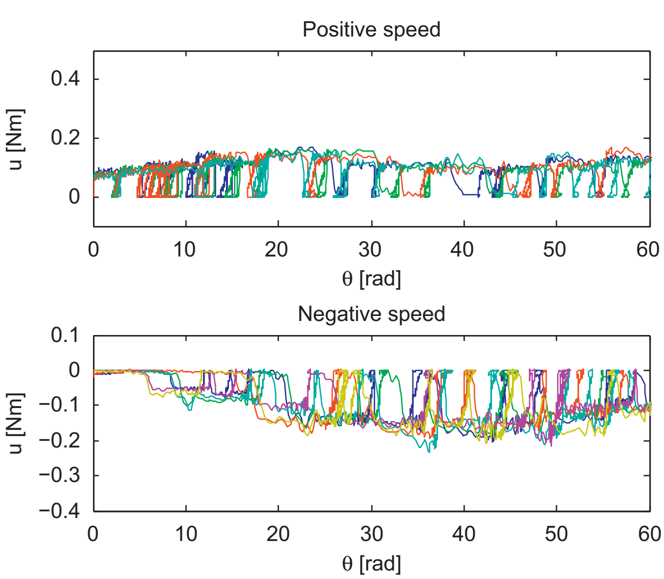

Fig. 14. Initial data obtained for the identification of C_s with the algorithm of Section 3.2.

Table 5
Parameters of the polynomial functions of C_s.

Parameters	Value	Parameters	Value
b_3^+	2.8731×10^{-6}	b_4^-	2.5120×10^{-7}
b_2^+	-2.7773×10^{-4}	b_3^-	-3.2940×10^{-5}
b_1^+	0.0077	b_2^-	0.0013
b_0^+	0.0794	b_1^-	-0.0126
		b_0^-	0.0938

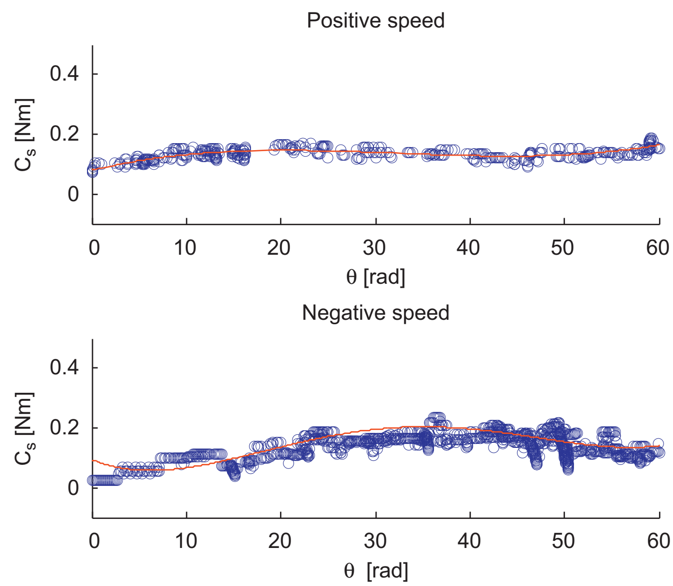

Fig. 15. Extremum and filtered C_s torques (circle), estimated Stribeck torque (solid).

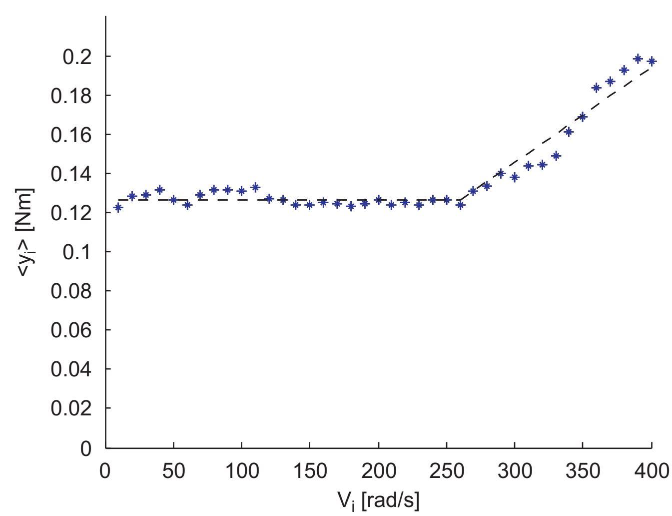

Fig. 16. Average results of the sinusoidal identification method: measured data (stars) and partial linear approximations (dashed line).

it appears that the assumption made in Eq. (31) of an affine frictions function is not accurate. For a velocity < 240 rad/s, $y(V_i)$ is constant thanks to dry friction. For higher speeds, viscous friction should be taken into account. To model the friction of the studied system, formulation (48) is used for viscous friction.

$$f_v(\omega) = 0 \text{ if } |\omega| < 240 \text{ rad/s} = f_v \text{ else} \tag{48}$$

The resistive torque C_r is given by

$$C_r(\theta,\mathrm{sign}(\omega)>0)=\frac{\overline{C_r^+}}{\overline{C_s^+}}C_s^+(\theta)=\frac{C_s^+(\theta)}{\beta^+}$$

$$C_r(\theta,\ \mathrm{sign}(\omega)<0)=-\frac{\overline{C_r^-}}{\overline{C_s^-}}C_s^-(\theta)=-\frac{C_s^-(\theta)}{\beta^-} \tag{49}$$

From the measured values of $\overline{C_s^+}$, $\overline{C_s^-}$, $\overline{C_r^+}$ and $\overline{C_r^-}$, it comes: $\beta^+=1.2325$, $\beta^-=1.3728$.

Using a simple least square algorithm, from Fig. 16 and Eq. (35), the viscous friction coefficient f_v and the mean Coulomb torque $\overline{C}_r$ are estimated to 7.1746×10^{-4} Nm/s and 0.1094 Nm. The identified friction function does not fit with usual friction function. This may come from the complex interactions between the different mechanical parts of the system. As it will be shown in the next section, the obtained unusual friction function permits to fit simulated and experimental tests.

5.3. Validation

In order to validate the identification work, a position test is applied to the test bench and to the model. The linear controller defined above is used again in closed loop. Figs. 17 and 18 present the results of the experimental test bench. Trajectories obtained with the model are given by Figs. 19 and 20.

Zoom of Fig. 21 shows that step response of the model is closed to the real system for θ and u. But the time period and the amplitude of the limit cycles are higher with the model. Moreover during these cycles, the model input torque is higher than the one of the real system. This difference is due to the non-modeling of the mechanical play when the system is stabilized near a constant position. Indeed, when limit cycles occurs, the mechanical play dissociates the rotor from the toothed rack. Then, the resistant torque is only equal to the one the motor.

The model is modified to take into account the mechanical play between the rotor and the toothed rack. From result of Fig. 18, the dry friction of the motor is estimated to be C_d=0.05 Nm. The Stribeck torque C_{ds} is set to 0.055 Nm. Results are presented in Fig. 22. Limit cycles are better modeled.

Generally, to remove limit cycles, the input torque is set to be 0 when the position is sufficiently closed to the desired value. In this case, it is useless to model precisely limit cycles. The first

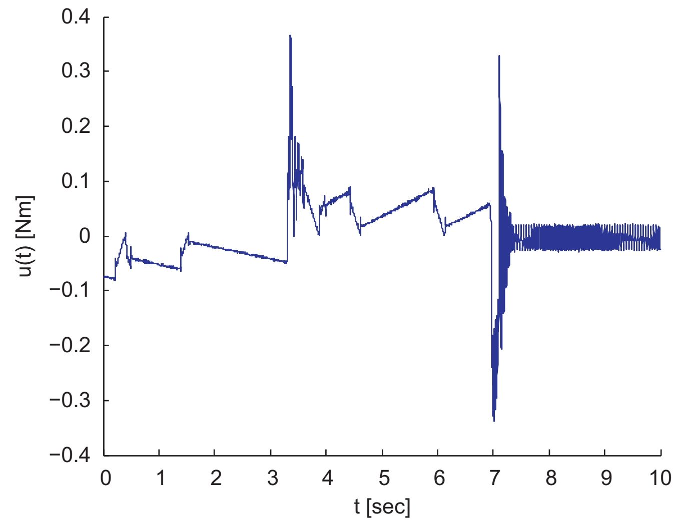

Fig. 18. Results of the position test applied to the experimental test bench: input torque $u(t)$.

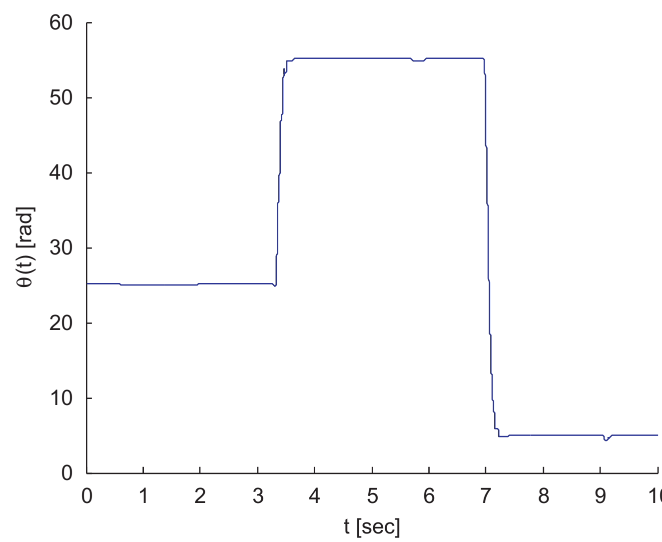

Fig. 19. Results of the position test applied to the model: measured position.

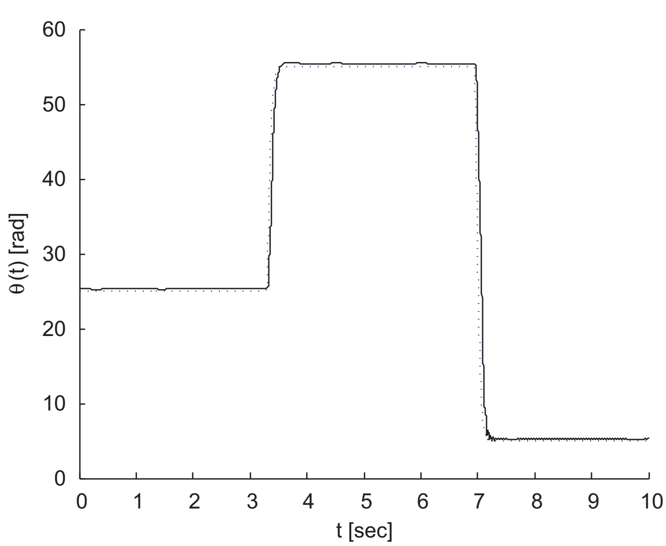

Fig. 17. Results of the position test applied to the experimental test bench: desired position (dashed), measured position (solid).

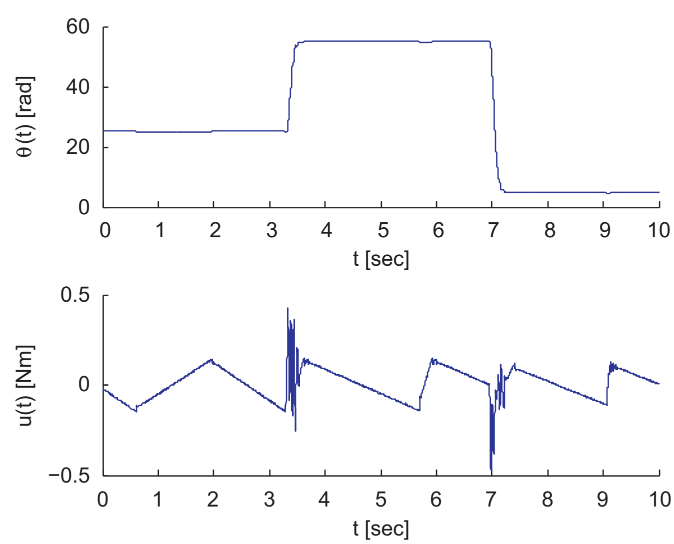

Fig. 20. Results of the position test applied to the model: input torque $u(t)$.

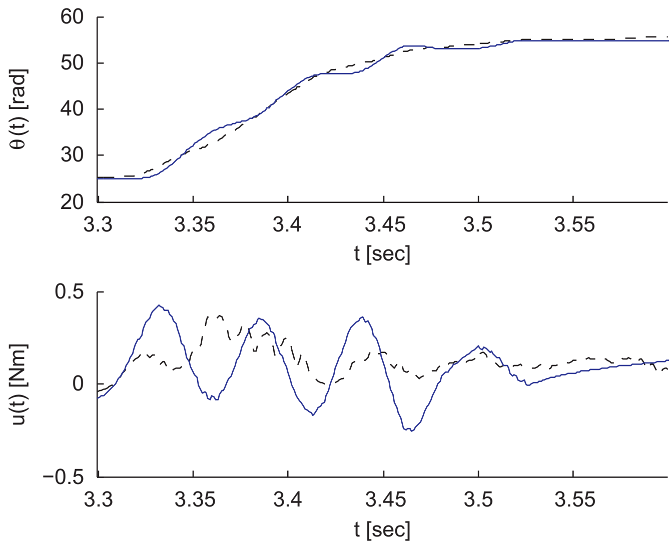

Fig. 21. Zoom: model (solid) and real system (dashed).

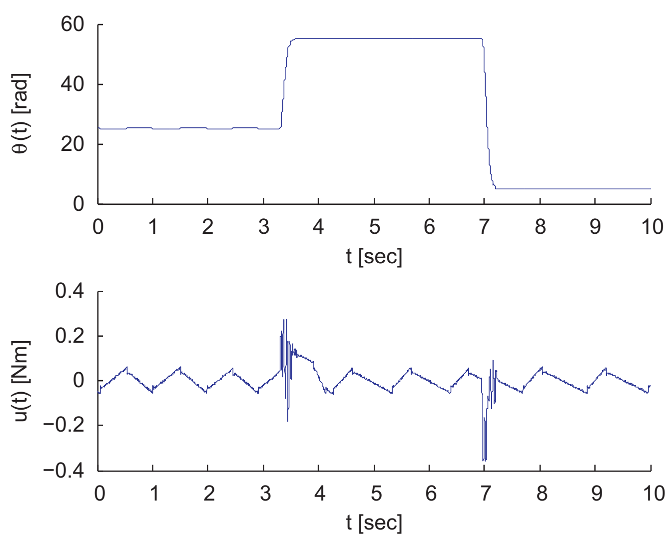

Fig. 22. Results with the modeling of mechanical play.

model without mechanical play is enough for the synthesis and the test of a control law.

6. Conclusion

This paper has presented a hybrid model with two states (modes) for system submitted to dry friction. The mode 0 models the system behavior during sticking motion and mode 1 describes slipping dynamics. Switch conditions depend on the input force and the speed. To ensure that no switch is missed by numerical integration, solver parameters conditions have been given.

The main advantage of the presented model is the adaptation capability of the model to observable phenomena. For example pre-sliding displacement can be taken into account or not. Following tests of Canudas de Wit et al. (1995) and Dupont et al. (2000), the performances of the hybrid one are equivalent or higher than the LuGre and the elastoplastic models. By splitting the system in two modes, each phenomenon can be studied and identified without interfere with the others. Moreover, the proposed model has nativelyy the no-drift property compared to the LuGre model, without additional parameters as the elasto-plastic model.

The model parameters are of two kinds: simulation and physical parameters. Inequalities have been set out for the first class to obtain accurate simulation results with a moderate simulation time. For the second one, a simple method has been described to find the values of the minimum set of physical parameters for hybrid model. First, the breakaway force f_s is found with a control input using stick–slip effect. Secondly, with a supposed known mass m, a method based on sinusoidal speed signal is used to find friction parameters f_c and f_v. If the noise of the measured input force u_s has a null average, there is no bias on the identified parameters. The method focus to search identifiable parameters (f_v and f_c) plus being robust to the unidentifiable parameter m (due to low resolution position sensor). This approach uses sinusoidal trajectories and can be applied to system with position limitation. Of course, more the speed trajectory fits with the sinusoidal reference, more the results will be efficient. The proposed parameters identification method can be used with other dry friction models than the hybrid one.

To valid the hybrid model and its identification method, a clutch-by-wire is studied. After the presentation of the system, simplifications have been done to obtain a single-mass system with dry and viscous frictions. This model is used to identify the set of parameters. The complex interactions between all the parts of the system involve a position dependance of dry frictions and a unusual viscous friction function.

7. Future works

Many ways of development should be found from the presented hybrid model and/or the studied clutch actuator. First, a solver may be developed to respect numerical integration conditions. Then, depending on mechanical system speed, integration step time would adapted and simulation time would be decreased.

Secondly, the last non-modeled phenomena as hysteresis behavior with nonlocal memory should be integrated using for example the Preisach model. Identification methods developed for electro-magnetism system should be used to identify Preisach model parameters.

Thirdly, the single-mass model of the studied clutch actuator has been formulated as a LPV system. From this formulation, a LPV controller robust to parameter uncertainties may be developed.

Acknowledgements

This work was supported by the ADEME (French Environment and Energy Management Agency) Grant #0566C 0009 under PREDIT (programme of research, experimentation and innovation in land transport) operational group #8.

References

Al-Bender, F., & Swervers, J. (2008). Characterization of friction force dynamics. *IEEE Control Systems Magazine*, 64–81.
Alpeter, F. (1999). *Friction modeling, identification and compensation*, Ph.D. thesis, Ecole polytechnique fédérale de Lausanne.
Alur, R., Henzinger, A., & Sontag, E. (1996). Hybrid systems iii: Verification and control. In *Lecture notes in computer science* (Vol. 1066).
Antsaklis, P. (2000). Special issue on hybrid systems: Theory and application. *Proceedings of IEEE*, *88*(7).
Antsaklis, P., Kohn, W., Nerode, A., & Sastry, S. (1995). Hybrid systems ii. In *Lecture notes in computer science* (Vol. 999).
Antsaklis, P., Kohn, W., Nerode, A., & Sastry, S. (1997). Hybrid systems iv. In *Lecture notes in computer science* (Vol. 1273).

Antsaklis, P., & Nerode, A. (1998). Special issue on hybrid control systems. *IEEE Transactions on Automatic Control*, *43*.
Armstrong-Helouvry, B., Dupont, P., & Canudas de Wit, C. (1994). A survey of models, analysis tools and compensation methods for the control of machines with friction. *Automatica*, *30*, 1083–1138.
Besancon-Voda, A., & Besancon, G. (1999). Analysis of a two-relay system configuration with application to coulomb friction identification. *Automatica*, *35*, 1391–1399.
Besancon-Voda, A., & Blaha, P. (2002). Describing function approximation of a two-relay system configuration with application to coulomb friction identification. *Control Engineering Practice*, *10*, 655–668.
Bliman, P., & Sorine, M., (1995). Easy-to-use realistic dry friction models for automatic control. In *Proceedings of third european conference*. Rome, Italy.
Canudas de Wit, C. (1999). Workshop on control of systems with friction. In *IEEEconference on control applications*. Hawaii, USA.
Canudas de Wit, C., Olsson, H., Astrom, K. J., & Lischinsky, P. (1995). A new model for control of systems with friction. *IEEE Transactions on automatic control*, *10*(3), 419–425.
Di Benedetto, N. & Sangiovanni-Vincentelli, A. (2001). Hybrid systems: Computation and control. In *Lecture notes in computer science* (Vol. 2034).
Dupont, P., Armstrong, B., & Hayward, V. (2000). Elastoplastic friction model: contact compliance and stiction. In *Proceedings of American control conference*. Chicago, IL.
Dupont, P., Hayward, V., Armstrong, B., & Altpeter, F. (2002). Single state elastoplastic friction models. *IEEE Transactions on Automatic Control*, *47*, 198–787.
Grossman, R., Nerode, A., Ravn, A., & Rischel, H. (1993). Hybrid systems. In *Lecture notes in computer science* (Vol. 736).
Henzinger, T., & Sastry, S. (1998), Hybrid systems: Computation and control. In *Lecture notes in computer science* (Vol. 1386).
Karnopp, D. (1985). Computer simulation of stick–slip friction in mechanical dynamic systems. *Journal of Dynamic Systems, Measurement and Control, Transactions ASME*.
Lampaert, V., Swervers, J., & Al-Bender, F. (2002), Modification of the leuven integrated friction model structure. *IEEE Transactions on Automatic Control*, 47, 683–687.
Lynch, N. & Krogh, H. (2000), Hybrid systems: Computation and control. In *Lecture notes in computer science* (Vol. 1790).
Maler, O. & Pnueli, A. (2003), Hybrid systems: Computation and control. In *Lecture notes in computer science* (Vol. 2623).
Mayergoyz, I. (1991). *Mathematical models of hysteresis*. New York: Springer-Verlag.
Morse, A., Panelides, C., Sastry, S., & Schumacher, J. (1999). Special issue on hybrid control systems. *IEEE Transactions on Automatic Control*, *35*(3).
Nouailletas, R. (2009). *Hybrid modeling, identification, command and state estimation of dry friction system—application to a clutch-by-wire*. Ph.D. thesis, Grenoble INP.
Nouailletas, R., Hoang Le, B., Mendes, E., & Koenig, D. (2008). New hybrid model and switched pi observer for dry friction systems. In *IFAC world congress*. Seoul, Korea.
Nouailletas, R., Mendes, E., & Koenig, D. (2008). Parameters identification of a hybrid model for dry friction. In *IEEE conference on decision and control*.
Sedghi, B. (2003). *Control design of hybrid systems via dehybridization*, École Polytechnique Fédérale de Lausanne.
Stribeck, R. (1902). Die wesentlichen eigenschaften des gleit-und rollenlager. *Zeitschrift des vereines seutscher ingenieure*, *46*(38,39), 1342–1348. 1432–1437.
Swevers, J., Al-Bender, F., Ganseman, C., & Projogo, T. (2000). An integrated friction model structure with improved presliding behavior for accurate friction compensation. *IEEE Transactions on Automatic Control*, *45*, 675–686.
Tomlin, C., & Greenstreet, M. (2002). Hybrid systems: Computation and control. In *Lecture notes in computer science* (Vol. 2289).
Vaandrager, F., & van Schuppen, J. (2000). Hybrid systems: Computation and control. In *Lecture notes in computer science* (Vol. 1569).
van der Schaft, A., & Schumacher, H. (2000). *An introduction to hybrid dynamical systems*. London: Springer-Verlag.
Witsenhausen, H. (1976). A class of hybrid-state continuous-time dynamic systems. *IEEE Transactions on Automatic Control*, *11*, 161–167.